A FEM-Matlab code for Fluid-Structure interaction coupling with application to sail aerodynamics of yachts

D. TRIMARCHI
FSI Group - University of Southampton, Southampton, UK (formerly MSc student at DINAV)
C.M. RIZZO
DINAV – Università degli Studi di Genova, Genova, Italy

ABSTRACT: A Matlab-FEM code has been developed for deformation analysis of sails as a MSc final project. Sails are modelled as isotropic homogeneous membranes reinforced with cables. The problem, fully non-linear, is resolved by assembling the global stiffness matrix of a mesh of membrane and cable elements in the Matlab™ environment to get an N-equations N-unknowns system. The solution is found with a Quasi-Newton solver. Validation has been performed by comparing numerical results obtained from the developed code with analytical solutions of geometrically simple cases and with experimental data from tests carried out in the DINAV Ship Structures laboratory. A full Fluid Structure Interaction (FSI) analysis of a main sail has been carried out coupling the code with an aerodynamics panel code developed as another MSc final project (Vernengo, 2008). The result is in accordance with the physics of the phenomena and engineering judgment.

1 INTRODUCTION

In recent years technological innovations have introduced large improvements in sail design and construction. The work of sail-makers is more and more becoming a high-tech job in collaboration with skilled aerodynamicists and material scientists, especially when dealing with the most competitive sailing teams. Competitions like America's Cup or Volvo Ocean Race are the best fields to improve optimisation processes. From those fields, studies have been developed widely and it's often possible to see high-tech sails even on cruising boats used for local yacht club regattas.

Furthermore, kites are nowadays becoming very popular, for both sport and as ships' auxiliary propulsion. Implementing this technology, a significant decrease (10-35%) on average annual fuel cost is claimed (www.skysails.info). This system seems to gain success and many articles can be found in open literature. Studies are ongoing into wind turbines, demonstrating that their efficiency is increased by the kite's ability to fly at high altitudes, not subjected to any wind gradient (www.kitegen.com).

This kind of study is very challenging due to the large number of different interactions. Sails are in fact a typical example of Fluid-Structure Interaction (FSI) and need very different engineering skills to be merged.

As a matter of fact, pressures generated by sails depend on the sail's equilibrium shape. The equilibrium shape is a function of the applied load (sum of pre-loads and aerodynamic loads), structural stiffness and boundary conditions, as for example battens and rigging.

The Finite Element (FE) tool described in this paper calculates the deformation of a sail loaded with a generic pressure load. The definition of loads has to be done by an external aerodynamic code analysing the wind flow over the deformed geometry of the sail.

2 STRUCTURAL METHOD

The method adopted for the sail-deformation calculation is the development of a finite difference code for 2-D beams used for teaching purposes (Carassale, 2007). Elements have been modified and are now 3D triangular isotropic homogeneous membranes and cable elements. Even if the assumptions adopted for this model are rather approximate, they have been considered acceptable as the starting point for future developments. On the other hand, cables can supply the lack of accuracy in the orthotropic materials and structural behaviour modelling. Actually, advanced sail-makers are using specific tools for sail design (e.g. Membrain - www.northsails.com , Relax - www.peterheppel.com , SA Evolution - www.smar-azure.com, SailFlex - www.yru-kiel.de) and the need to get more accurate results is represented in a continuous development of such codes. However, no specifically developed codes are available in open literature as existing ones are considered commercially sensitive.

In the past, various papers have been presented on the modelling of sail structural behaviour, but often sails have been discretised with cables or beam systems, i.e. mono-dimensional elements (Hauville, 2004; Fantini, 2004). However, membrane structural behaviour has been studied for different purposes and in other engineering fields.

After a rather comprehensive literature review on the definition of membrane elements for FE codes, the elements implemented in the present work have been derived from the ones originally defined by Li and Chan (2004). In their article they further developed previous works by Tabarrok and Qin (1992) and Levy et al. (2004). Elements stiffness matrices are explicitly expressed in terms of geometric global coordinates of the nodes of the elements and of the material properties, so they are very straightforward to implement in a self-developed FE code.

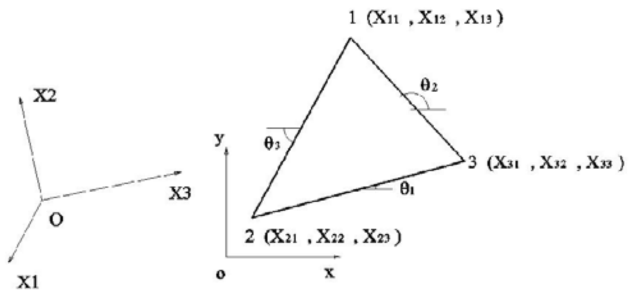

Figure 1. Element geometrical definition.

The basis of the FE theory is the Principle of Virtual Works (PVW), discretised and expressed in matrix form. Li and Chan's paper proposes an element stiffness matrix composed by an elastic stiffness matrix (linear) plus a geometric stiffness matrix (nonlinear):

$$\mathbf{K} = \mathbf{K}_E + \mathbf{K}_G \qquad (1)$$

where $\mathbf{K}$ =Global Stiffness Matrix, $\mathbf{K}_E$ = Elastic Stiffness Matrix, $\mathbf{K}_G$ = Geometric Stiffness Matrix.

Physically, the stiffness matrix expresses a relationship between external applied loads and nodal displacements caused by applied loads and is a linear operator. For large displacement analysis, the problem becomes non-linear since the structure's stiffness (necessary to calculate displacements) is not defined *a priori* but it has to be calculated as a function of nodal displacements. The problem is generally solved with an iterative procedure.

For the implemented elements the elastic stiffness matrix is defined as:

$$\mathbf{K}_{\mathbf{E}} = A \cdot t \cdot \mathbf{T}_{\mathbf{G}}^{\mathbf{T}} \cdot \mathbf{T}_{\mathbf{N}}^{\mathbf{T}} \cdot \mathbf{D} \cdot \mathbf{T}_{\mathbf{N}} \cdot \mathbf{T}_{\mathbf{G}} \qquad (2)$$

where l_{0ij} are the length of the undeformed element sides and $A \cdot t$ is the undeformed element volume. Also, with reference to Fig. 1:

$$\mathbf{T}_{\mathbf{G}} = \begin{bmatrix} 0 & 0 & 0 & -\alpha_{23} & -\beta_{23} & -\chi_{23} & \alpha_{23} & \beta_{23} & \chi_{23} \\ \alpha_{31} & \beta_{31} & \chi_{31} & 0 & 0 & 0 & -\alpha_{31} & -\beta_{31} & -\chi_{31} \\ -\alpha_{12} & -\beta_{12} & -\chi_{12} & \alpha_{12} & \beta_{12} & \chi_{12} & 0 & 0 & 0 \end{bmatrix}$$

$$\alpha_{ij} = \frac{X_{j1} - X_{i1}}{l_{0ij}} \; ; \; \beta_{ij} = \frac{X_{j2} - X_{i2}}{l_{0ij}} \; ; \; \chi_{ij} = \frac{X_{j3} - X_{i3}}{l_{0ij}}$$

$$\mathbf{T}_{\mathbf{N}} = \mathbf{\Psi}^{-1} \cdot \mathbf{L}_{\mathbf{0d}}^{-1}$$

$$\mathbf{\Psi} = \begin{bmatrix} \cos^2\theta_1 & sen^2\theta_1 & sen\theta_1 \cos\theta_1 \\ \cos^2\theta_2 & sen^2\theta_2 & sen\theta_2 \cos\theta_2 \\ \cos^2\theta_3 & sen^2\theta_3 & sen\theta_3 \cos\theta_3 \end{bmatrix}$$

$$\mathbf{L}_{\mathbf{0d}} = \begin{bmatrix} l_{023} & 0 & 0 \\ 0 & l_{031} & 0 \\ 0 & 0 & l_{012} \end{bmatrix}$$

$$\mathbf{D} = \frac{E}{1-\nu^2} \cdot \begin{bmatrix} 1 & \nu & 0 \\ \nu & 1 & 0 \\ 0 & 0 & \frac{1-\nu}{2} \end{bmatrix}$$

The geometric stiffness matrix is defined as:

$$[\mathbf{K}_G] = \begin{bmatrix} \mathbf{B}_{12} + \mathbf{B}_{31} & -\mathbf{B}_{12} & -\mathbf{B}_{31} \\ -\mathbf{B}_{12} & \mathbf{B}_{12} + \mathbf{B}_{23} & -\mathbf{B}_{23} \\ -\mathbf{B}_{31} & -\mathbf{B}_{23} & \mathbf{B}_{23} + \mathbf{B}_{31} \end{bmatrix} \qquad (3)$$

where $\mathbf{B}_{\mathbf{ij}} = \frac{\mathbf{P}_{\mathbf{ij}}}{\mathbf{l}_{\mathbf{ij}}} \cdot \left[\mathbf{I}_3 - \mathbf{C}_{\mathbf{ij}} \cdot \mathbf{C}_{\mathbf{ij}}^{\mathbf{T}}\right]$; $\mathbf{P}_{\mathbf{ij}}$ = tension between nodes i , j ; $\mathbf{I}_3$: Identity Matrix [3x3] ;

$$\mathbf{C}_{\mathbf{ij}} = \frac{1}{l_{0ij}} \left\{ (X_{j1} - X_{i1}) \cdot (X_{j2} - X_{i2}) \cdot (X_{j3} - X_{i3}) \right\}^T$$

While for cable elements:

$$[\mathbf{K}_e]_{CABLE} = \frac{EA}{l_0} \begin{bmatrix} \mathbf{C} \cdot \mathbf{C}^T & -\mathbf{C} \cdot \mathbf{C}^T \\ -\mathbf{C} \cdot \mathbf{C}^T & \mathbf{C} \cdot \mathbf{C}^T \end{bmatrix} \qquad (4)$$

where: $\mathbf{C}_i = \frac{1}{l_0} \left(X_{IIi} - X_{Ii} \right)$

$$[\mathbf{K}_G]_{CABLE} = \frac{T}{l_0} \begin{bmatrix} \mathbf{I}_3 - \mathbf{CC}^T & -(\mathbf{I}_3 - \mathbf{CC}^T) \\ -(\mathbf{I}_3 - \mathbf{CC}^T) & \mathbf{I}_3 - \mathbf{CC}^T \end{bmatrix}$$

(5)where: T is the cable tension.

Once both element's stiffness matrices are known, it is possible to assemble the global stiffness matrix $[\mathbf{K}]^{GLOB}$ as the sum of $\mathbf{K}_E$ and $\mathbf{K}_G$, which is now able to consider both elements contributions. Assembly is undertaken with proper Kronecker's tensors, built up in order to position nodal stiffness values in the correct position of the global stiffness matrix as follows:

$$[\mathbf{K}]^{GLOB} = \sum_{i=1}^{Ni} \mathbf{O}_i^T \cdot \left(\mathbf{K}_E^i + \mathbf{K}_G^i\right) \cdot \mathbf{O}_i \qquad (6)$$

where: $\mathbf{O}_i$ is the element's Kronecker tensor.

Once the global stiffness matrix $[\mathbf{K}]^{GLOB}$ is evaluated, it is possible to extract the stiffness matrix of free nodes $\mathbf{K}_{LL}$. This allows the definition of an N-equations N-unknowns system to be solved with a Quasi-Newton solver which is able to minimise the first term of the following equation:

$$\mathbf{K}_{LL} \cdot \mathbf{u}_L - \mathbf{P}_L = 0 \qquad (7)$$

where: $\mathbf{K}_{LL}$ = free nodes stiffness matrix; $\mathbf{u}_L$ = free nodes displacement vector; and $\mathbf{P}_L$ = applied loads on free nodes vector.

Three non-linearities are implemented in the Code:

NL1_ The Geometric Stiffness Matrix $\mathbf{K}_\mathbf{G}$ is non-linear, since it is defined as a function of the element's nodal displacements.

NL2_ is due to large displacements: loads (defined as discretised pressure load, i.e. force on nodes) have to be rotated in order to remain perpendicular to the deformed membrane.

NL3_ Material behaviour is non-linear, since membranes and cables are not reacting to compressive loads. In order to calculate the geometric stiffness matrix, when calculated tensions are negative they will be considered equal to zero in the iteration step and in the subsequent ones.

As shown in Fig. 2, the calculation is stabilised with a relaxation routine, which is able to smoothen numerical instabilities affecting the calculation during iterations on the geometric stiffness matrix. The relaxation is simply obtained by averaging the increase of nodal displacements at each step *i* by:

$$\mathbf{u}(i) = \frac{(\mathbf{u}(i-i) + \mathbf{u}(i))}{2} \qquad (8)$$

where: $u(i)$ = Nodal displacements at *i-th* iteration

In order to stabilise numerical results it has been observed that the convergence curve (assumed as the norm of nodal displacements sum) oscillates rather symmetrically over the final result (Fig. 3). The convergence has been forced imposing calculated displacements on the *i-th* iteration as an average between displacements calculated on the *i-th* and *(i-1)-th* iteration.

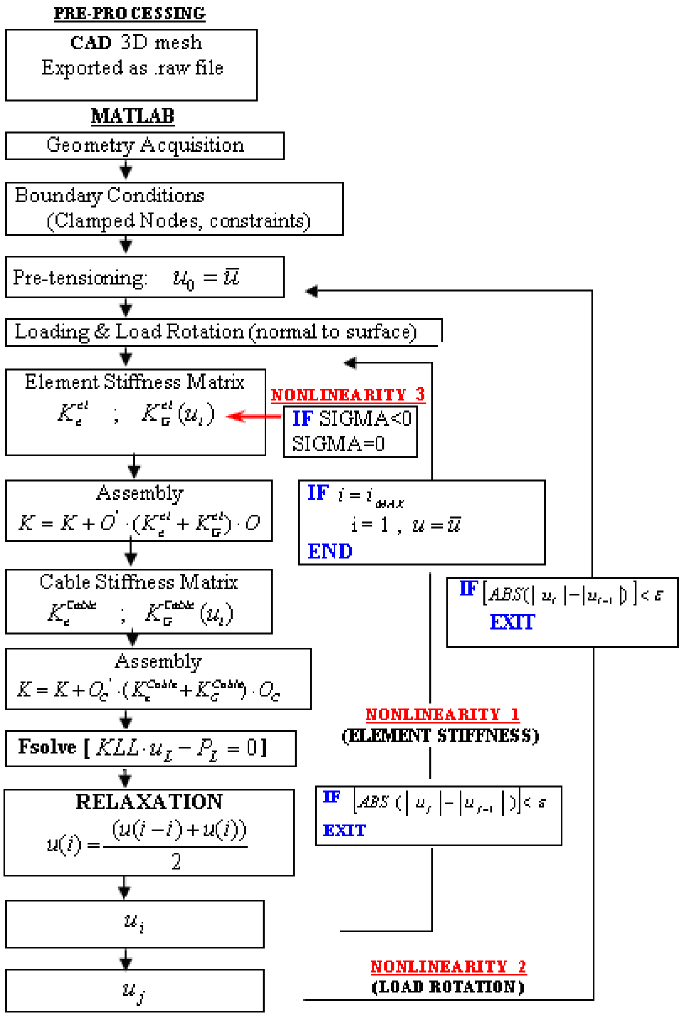

Figure 2. The flow chart of the calculation

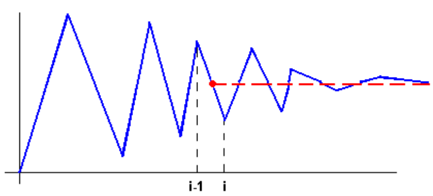

Figure 3. Convergence behaviour

3 ANALYTICAL COMPARISON

Code validation has been performed first comparing analytical results with numerical results. Later on, an experimental validation has been performed.

The first analysis regards a holed membrane in tension. The analytical results are well known in terms of displacements and stresses and the stress concentration factor is 3.0 at hole's quadrants. Analysis has been performed using three different meshes, adapting element size around the hole. A rather significant mesh-sensivity was experienced, but results are acceptable once the mesh is properly refined according to usual engineering judgment.

In the test case, the membrane is 16mm wide and 1mm thick. It is loaded with 17 concentrated loads of 100N each. The material Young Modulus is $1000 N/mm^2$.

Therefore far-field stresses will be $\sigma = 106.25 \dfrac{N}{mm^2}$ and maximum nodal displacement $\varepsilon = \dfrac{\Delta\ell}{\ell_0} = \dfrac{\sigma}{E} = 0.10567 \Rightarrow \Delta\ell = 0.10567 \cdot \ell_0 = 1.69\, mm$.

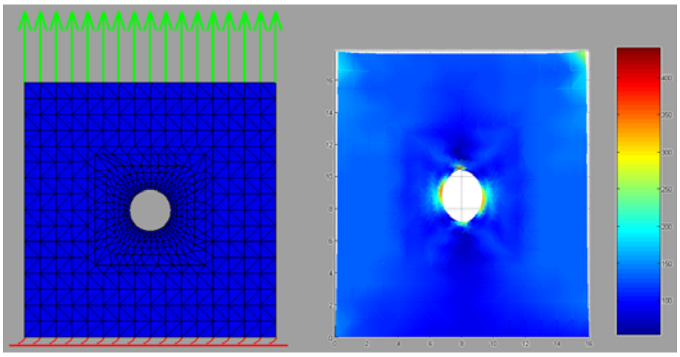

Figure 4. Adopted mesh and results in term of tension stresses

Numerical analysis gives displacements of about 1.64mm and the error is approximately 3%. Calculated far-field stress is about 105.9 N/mm^2 with an error of approximately 0.3%. Neglecting some numerical residuals, the stress concentration factor is 2.9 at hole's quadrants in tension and the error is approximately 3%.

Instability of elements in compressed areas of the hole is also noted (Fig. 5).

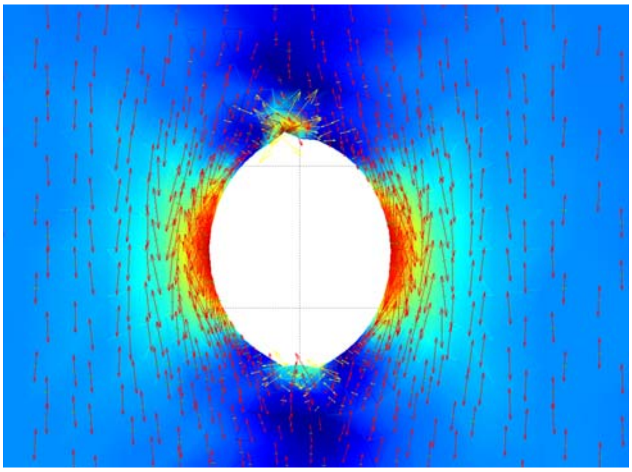

Figure 5. Zoom on the hole and principal stresses

Such results can be explained bearing in mind that in the code no model for wrinkling has been included. This assumption has been made in order to simplify the code in a first step of its development. On the other hand in the future a wrinkling model will be included in order to increase the accuracy of the calculation. In fact, as it is possible to see in Fig. 6, wrinkling can be significant in membrane deformation. In the literature many interesting references can be found, both in theoretical papers (Stanuszek, 2003; Lee, 2006; Diaby, 2006) and in some sail analysis devoted papers (Heppel, 2002).

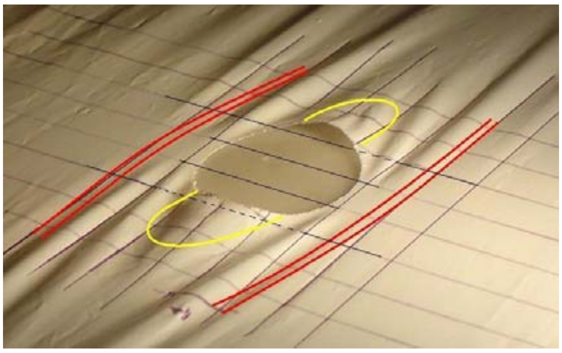

Figure 6. Wrinkling test

Without a wrinkling model able to deal with out-of-plane deformations, elements at the upper and lower quadrant of the hole are compressed but unable to react. This happens since the definition of the element's stiffness matrix does not deal with negative stresses (NL3). Therefore, compressed elements are "collapsed" in the plane and this can cause a large nodal displacement, as shown by the test of Fig. 6.

In the following, a sphere loaded with internal pressure has been analysed. The analytical solution is known and it is reported in the following. The increase in sphere-radius can be calculated as:

$$R' - R = \frac{1-\nu}{2 \cdot E \cdot t} \cdot P \cdot R^2 \qquad (9)$$

Due to the sphere symmetry, circumferential and tangential stresses will be equal and calculated as:

$$\sigma_\theta = \sigma_\varphi = \frac{P \cdot R^2}{2 \cdot t} \qquad (10)$$

In the test case it has been assumed:

$$R = 5\ mm \ ;\ t = 1\ mm$$
$$P = 100\ N/mm^2$$
$$E = 1000\ N/mm^2$$

Therefore expected results will be:

$$R' = 5.94\, mm$$
$$\sigma = \sqrt{\sigma_\theta^2 + \sigma_\varphi^2} = 354\ N/mm^2$$

As far as both deformation and stress is concerned, the numerical calculation gives rather accurate results: radius R' is in fact 5.97mm. The error is approximately 0.5%.

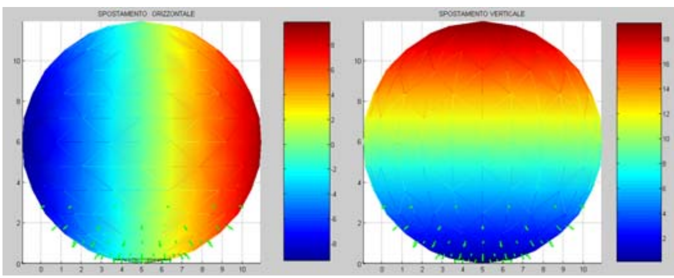

Figure 7. Nodal displacements

The stress value oscillates between $350 - 360 \frac{N}{mm^2}$ with the corresponding error being about 2.5%.

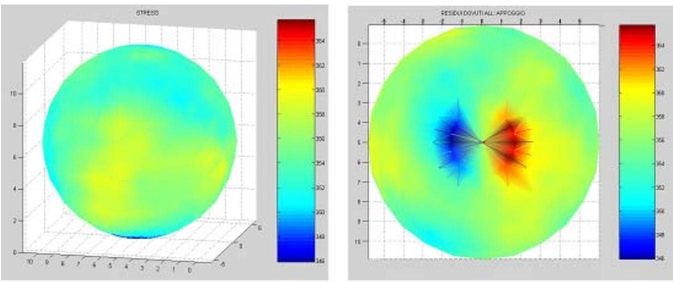

Figure 8. Stress values

The error value increases (up to 5%) on the clamped node at the base of the sphere (Fig. 8). Even if the sphere is not loaded by any own-weight load, the symmetry of the stress increase in this zone is noticeable. Actually, the explanation is that some numerical residuals would have brought the structure to a deformation which is not exactly symmetrical. The following reaction is supported by the only clamped node at the base, thus correcting the error caused by residuals. This causes a small distortion in the stress field. In fact, the value of the boundary reaction is 326 N, i.e. 4% of total load. This value is in agreement with the error already found for stresses.

Thereafter, a cylinder has been loaded with internal pressure as follows: $R = 2.5\ mm$; $t = 1\ mm$; $P = 100\ N/mm^2$; $E = 1000\ N/mm^2$

From the analytical solution it was found that:

$$u_R = \frac{P \cdot R^2 \cdot (1-\nu^2)}{E \cdot h} = 0.568\ mm$$

$$\sigma_\theta = R \cdot P = \frac{E}{1-\nu^2}\left(\frac{u_R}{R} + \nu \frac{du_z}{dz}\right) = 250\ N/mm^2 \qquad (25)$$

$$\sigma_z = 0$$

Numerical results obtained are again acceptable, in fact radial displacements are about 0.562mm. The error is 4%.

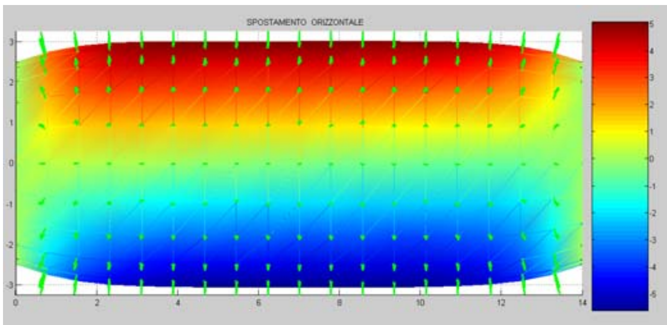

Figure 8. Nodal displacements

Calculated stress is $245\ N/mm^2$, the error is 2%.

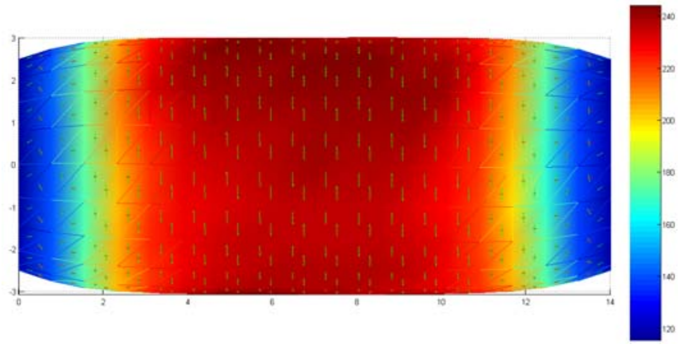

Figure 9. Principal stresses

4 EXPERIMENTAL MEASUREMENTS

Validation is continued comparing numerical data with experimental measurements. Two different experimental campaigns have been carried out. The first one was intended to measure the material's mechanical properties to be used in the calculation. The second one was intended to measure deformation of a flat membrane loaded with constant pressure.

Some tension tests have been carried out in order to find the stress-strain curve, i.e. the Young Modulus for 5 different sail materials. The weight of the sail fabric is generally measured in "sail maker's ounces" (smOz) where 1smOz = $43.3\ g/m^2$. For fibre-reinforced material, the currently adopted unit is the Denier per Inch (Dpi). This is the number of fibres per every inch in the warp direction. A second value is sometimes reported for the fill direction. In the present case, tested materials are: Dacron (7.5 smOz, 0° and 90°); Spinnaker's Nylon (1.5 smOz, 0° and 90°); Mylar and Kevlar (19 Dpi). The latter has been assumed isotropic.

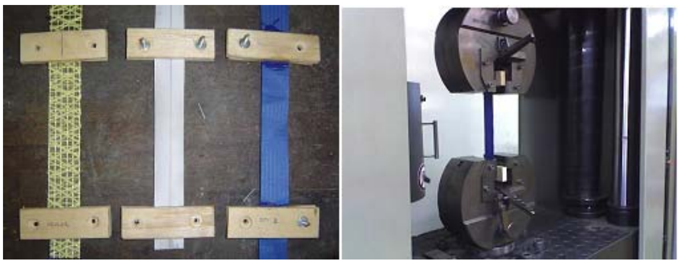

Figure 10. Traction tests

Measurements have been performed with laboratory machines for tension tests, able to obtain the force-displacement curve (Fig. 10).

From those tests, the Young Modulus of fabrics has been estimated considering the linear part of the plot and disregarding the initial and final parts of the curves, as reported in Fig. 11 and Table 1.

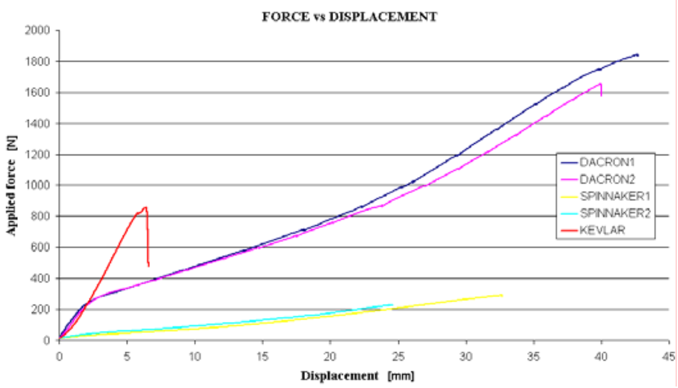

Figure 11. Force-Displacement curves

Table 1. Material properties

E	N/mm^2
Dacron (ortotropic) tested @ 0°	1667
Dacron (ortotropic) tested @ 90°	1712
Spinnaker (ortotropic) tested @ 0°	294
Spinnaker (ortotropic) tested @ 90°	458
Kevlar (isotropic)	1935

In order to test the accuracy of the code, the deformation of an initially flat Dacron membrane loaded with constant pressure has been measured. This test has been designed in order to assess the code's behaviour in a limit case, where the expected error is rather large. In fact, since the initial structure is flat, the elastic stiffness matrix is singular. The accuracy of the solution for very small deformations can therefore be expected not to be very accurate. On the other hand, the curvature of the structure is dramatically changing, from zero to larger values.

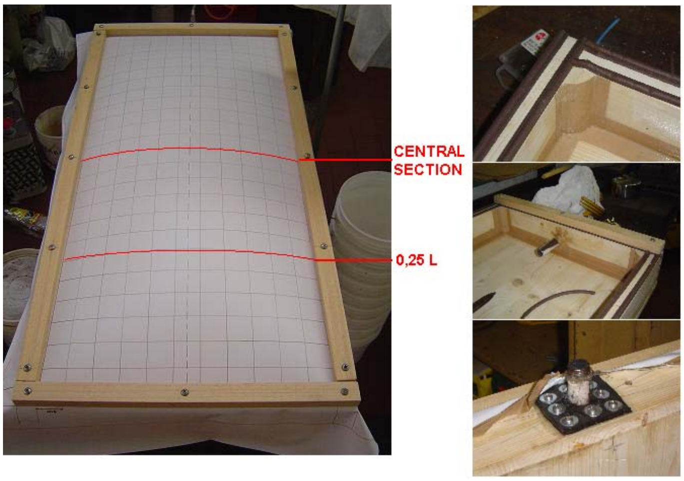

Figure 12. Box for deformation test

A wooden box has been built and a Dacron membrane has been fixed on the top (Fig. 12). The box has been made air-proof by a gasket and a special paper on the edges, normally used for the construction of church organs. The Dacron fabric has been fitted onto the box with fibres oriented along the box directions.

Compressed air has been pumped into the box and the pressure has been measured by water columns, providing very accurate measurements (Fig. 13) in the range of interest (11 to 88 cmH_2O i.e. 10 – 80 mbar).

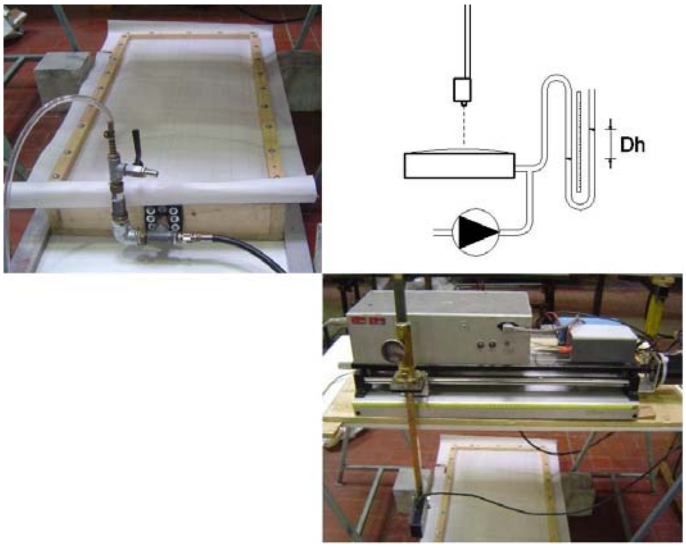

Figure 13. Measurement System

A laser device, able to measure distances, has been used to obtain the fabric deformations. Measurements have been carried out for 6 pressures in the range of interest. For some pressure values, deformation of 6 box's sections has been measured from the centre of the box. The data oscillations reported in Fig. 14 are probably due to noise (vibrations of the compressor, electromagnetic interferences on the measurement system, etc.). It has however been judged acceptable and have been smoothed by a 2nd order polynomial interpolation.

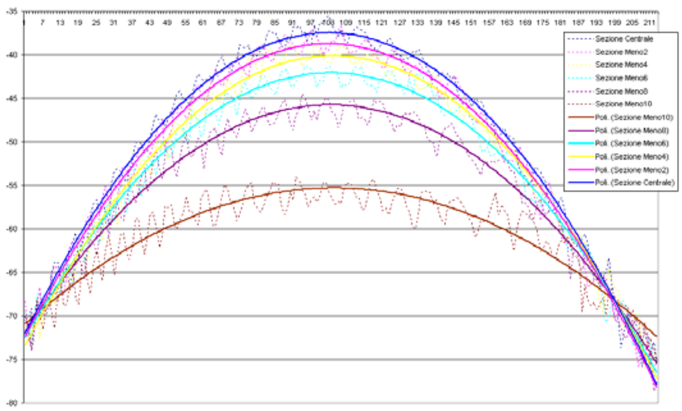

Figure 14. Measured deformed sections

Once the deformed shapes and material elastic properties were known, a comparison between numerical and experimental results was carried out. This was done for two sections (see Fig. 15) and for six different pressures in the range of interest.

A 784 element mesh has been adopted (Fig. 15) and the FE deformed shape seems rather different compared to the experimentally deformed one, especially at midspan. The calculated shape doesn't look smooth as in the experimental one, as the sections remain flat near the edges and suddenly bend in the centre. Also, caused by the low value of the initial curvature, vertical displacement of the nodes is magnified in the centre of the membrane, providing an important source of error.

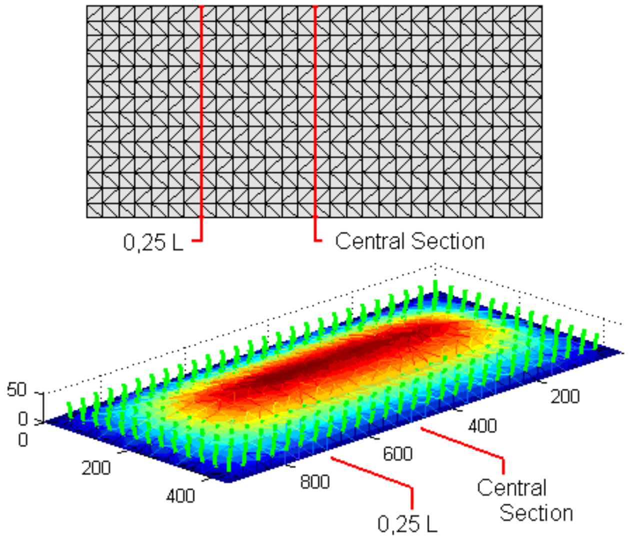

Figure 15. Numerical results of box test

In Fig. 16 (left) the comparison for the central section loaded with an 88cm water column (0.086 bar) is reported. The error is maximum at membrane's centre, i.e. in the most distant point from fixed edges and where curvature is smallest.

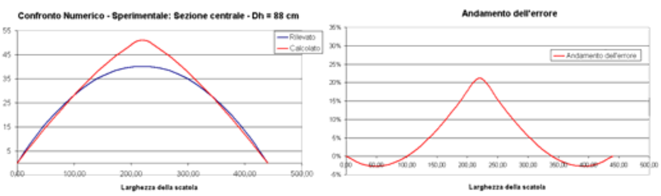

Figure 16. Measured vs computed results and error values

In Fig. 17 the graph reports a response surface of the error for six different tested pressures at central section and at @0,25L section. Therefore Fig. 17 reports the same values as Fig. 16 (right), but for many different tested pressures. This graph shows the error value is largest at the centre and it takes larger values for section @0,25L where final-curvature is lower. The error does not show a strong dependency on applied pressure.

It is worth pointing out that such error is not due to the Quasi-Newton solver converging to a local minimum. In fact, modifying the initial curvature of the membrane does not appear to be relevant for the final result. Similarly, the mesh refinement does not seem to influence the results: using an 1196 element mesh, finer in the central zone of the membrane, the error values decreases by about 1%. It is not easy to explain the origin of such an error, and in the future this subject will need more attention.

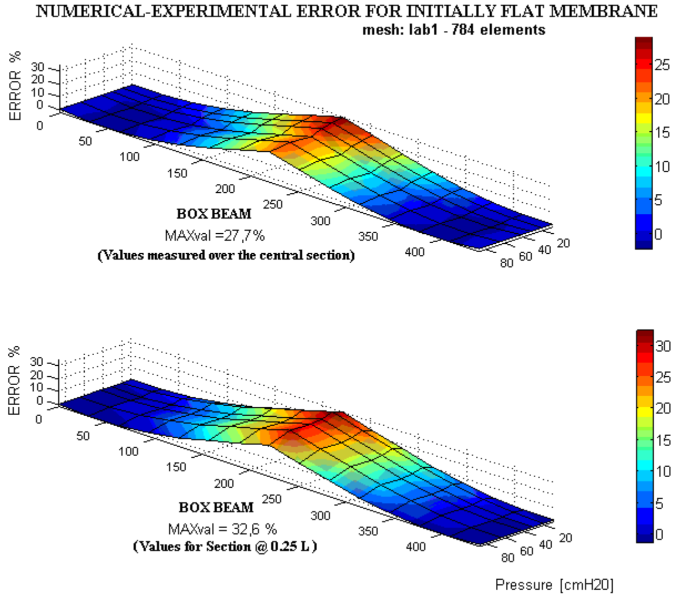

Figure 17. Error value for different pressures

5 QUALITATIVE RESULTS

In the following, some additional comparisons are reported for cases whose analytical solution is not known. Validation is based on qualitative judgment of results. A cylinder loaded with very high internal pressure is studied first. In the first iteration of the calculation, Loads are radial and deformation is consequently found to be radial:

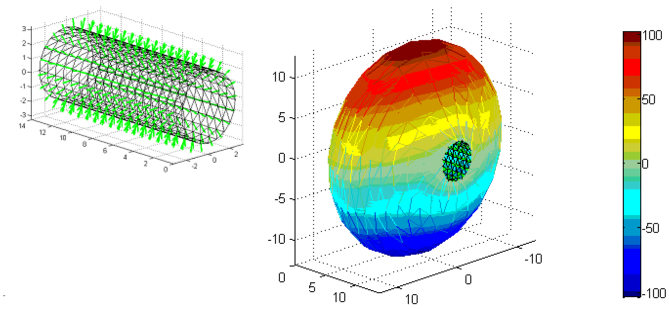
Figure 18. First iteration of cylinder in high pressure

Loads are rotated in subsequent iterations according to large displacement theory and the deformation shown in Fig. 19 seems to be consistent. Lateral edges are in fact rotated as shown:

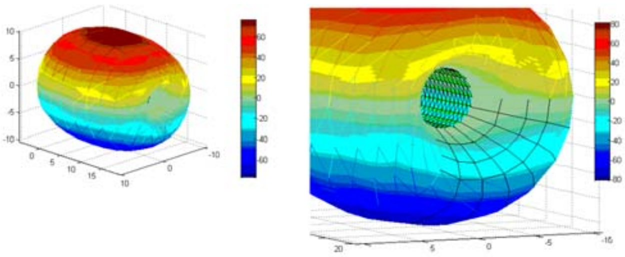
Figure 19. Equilibrium shape of cylinder in high pressure

Then, a spinnaker in sailing conditions has been analysed. The fabric has been loaded with a constant pressure equivalent to a 14 knots wind speed (3mbar). The Young's modulus is calculated as the average of the 2 measured values (Table 1, @0° and @90°) i.e. 375 N/mm^2. In the "design shape" the sail is 6000 mm high, the chord is 3750 mm and the max camber is 1670 mm. Some cable elements have been assembled on the foot, leech and luff of the sail. The results can be considered globally consistent, but the uncertainty is rather high, especially in the area of clew and tack. In those zones the increase in fabric thickness, due to additional layers sewn as reinforcement, has not been taken into account.

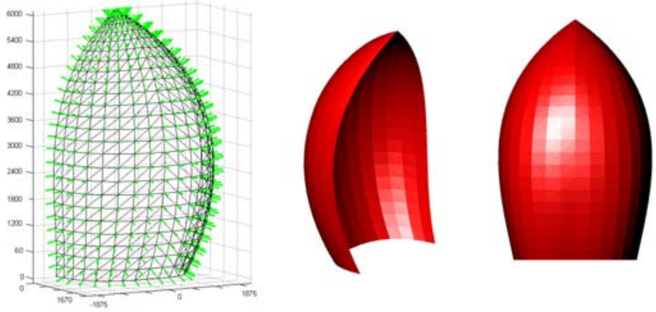

Figure 20. Spinnaker's design shape

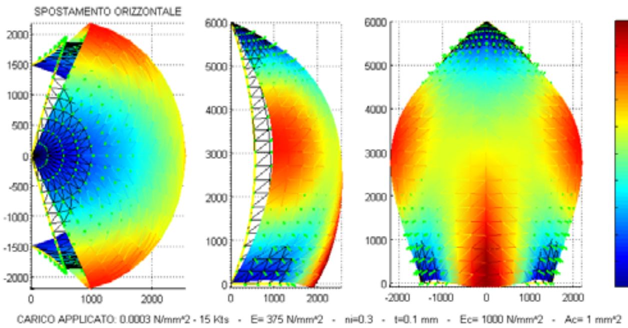

Figure 21. Nodal horizontal displacements

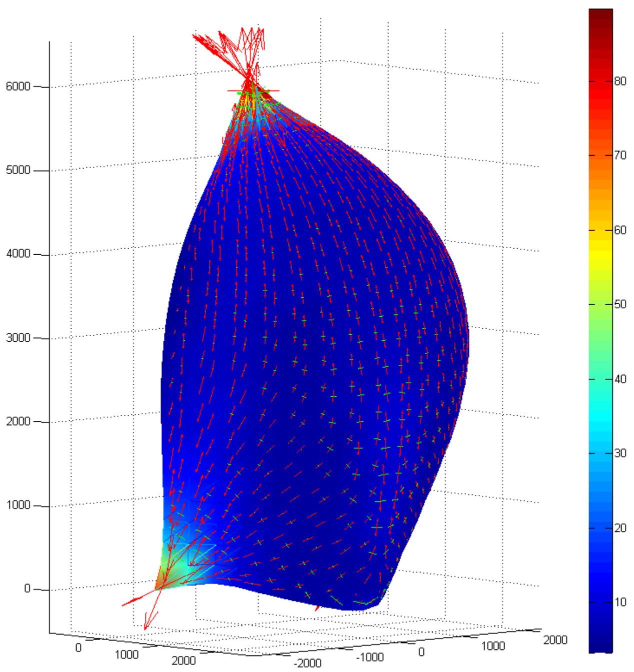

Figure 22. Principal stresses on spinnaker

Finally, a mainsail has been loaded with constant pressure equivalent to a 15 knots wind. Deformation seems to be consistent both in terms of nodal displacement and tension. It should be remarked that at this stage of the analysis the sail has not been pre-loaded, thus explaining the low value of tension on the head of the sail:

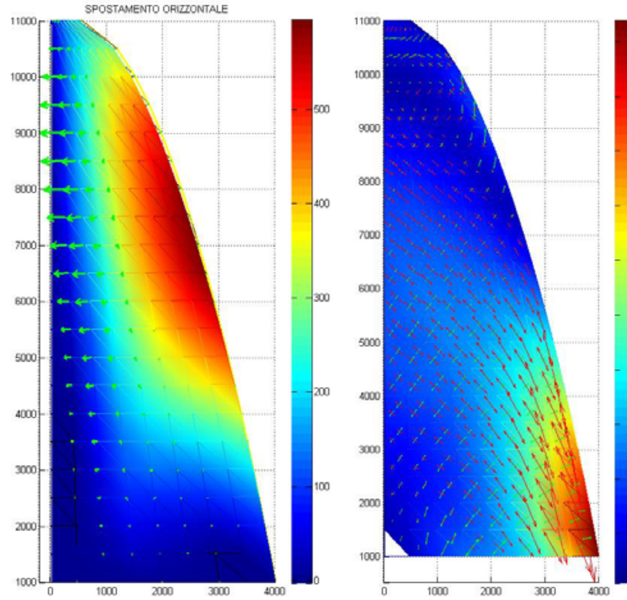

Figure 23. Nodal displacement and principals stresses

6 FLUID-STRUCTURE INTERACTIONS

An aerodynamic method has been developed to estimate loads on sails in a parallel MSc final project (Vernengo, 2008). It consists of a Vortex Lattice Method, able to calculate the circulation field, i.e. the pressure over a sail subjected to a wind flow. As a potential code, its validity is limited "close hauled course". The Fluid Structure Interaction (FSI) analysis has been carried up over a mainsail 12m high, with a chord of 5m, sailing upwind with a wind speed of 15 knots.

Coupling has been performed as follows: once the initial sail geometry X_0 (design shape) is defined, the aerodynamic code calculates pressure p_0 assuming a rigid profile. Pressure values are then passed to the structural code (present work) which defines the deformed geometry X_1. The latter is introduced again in the aerodynamic code, in order to calculate new pressures p_1, used in turn to deform the initial design shape X_0 and to calculate a new deformed geometry X_2. It is worth noting that structural analysis is always performed for the same initial geometry X_0, loaded by an updated pressure's field. X_0 is in fact the "design shape", i.e. the sail shape as built by the sail maker.

The procedure continues until achievement of a convergence criterion, based on the evaluation of the nodal displacement modulus, as in Fig. 26. In the present case, the sail was subjected to a parabolic wind profile, reaching a maximum velocity value of 20kts. The wind velocity vector presents a linear twist from the sea surface to the mast head, where it reaches its maximum value (45°). Since the sail has a variable geometric twist, the angle of attack has locally variations along the mast, given by the combination of geometric and aerodynamic twist. From a structural point of view, the fabric is described as:

$$Young\ \ Modulus : 1700\ {}^{N}\!\big/_{mm^2}$$

$$Fabric\,Thickness : 0.32\ mm$$

$$Poisson\ Ratio : 0.3$$

$$Cable\ Section\,(over\ the\ Leech) : 1\ mm^2$$

A very satisfactory convergence has been achieved in 13 iterations (error less than 1%):

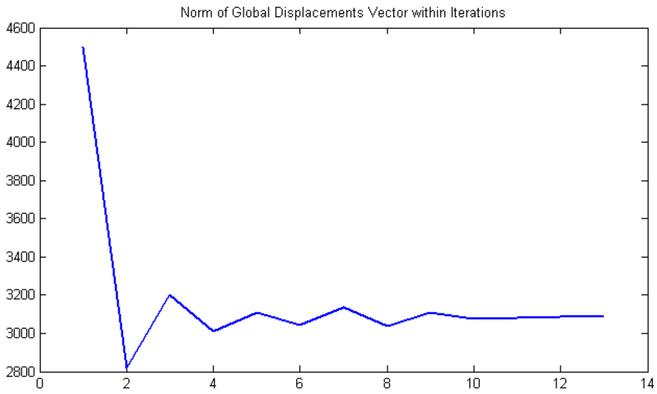

Figure 26. FSI convergence

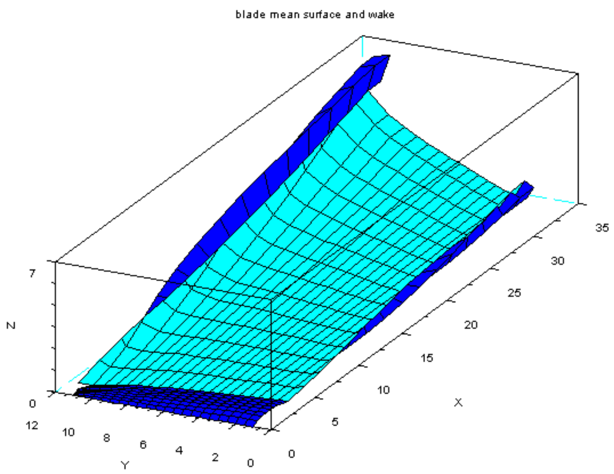

Figure 27. Aerodynamic Calculation

In Fig. 27, the behaviour of the wake developed from the sail in the equilibrium configuration is shown, and in Fig. 28 the corresponding sail deformation, shown laterally, from top and from aft, rotated 90° clockwise. Nodal loads deriving from calculated pressures are represented by arrows.

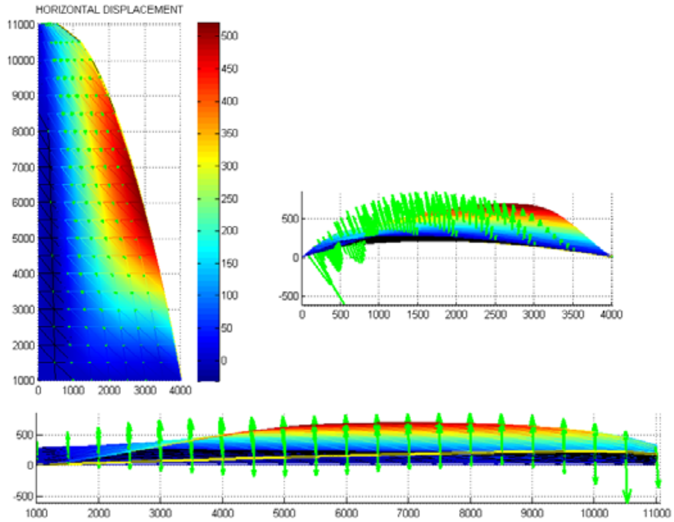

Figure 28. Final deformed shape (color map of deflections)

7 FUTURE DEVELOPMENT

The developed FEM method adopts many assumptions, which have been accepted as a starting point for future development.

Implemented elements are membranes and cables. In the future, battens will be included as a very important element for sail deformation analysis. In the present code, battens have been neglected since the implementation would require large programming effort but only offers small conceptual improvements. In fact, membranes and cables are both defined with three degrees of freedom at nodes, i.e. no bending strength. In order to include battens all nodes will have to pass from three to six degrees of freedom (DOF), thus modifying the architecture of the whole code. Moreover, the additional DOF should be coupled with membranes' nodes which by definition do not have bending DOF. On the other hand, completing the code makes it possible to take into account the rigging, which has a large influence on sail deformation.

The elements used are isotropic homogeneous membranes. In the future, an important development will be to implement some anisotropic elements with variable thickness, in order to simulate more accurately sail-making materials and the stiffened zones close to the sail's corners. Cable elements will be used also for the correct modelling of fibres included in the sail, as in modern sail materials (Fig. 10).

As described in Section 3, no wrinkling model has been included into the code, even if wrinkling is a quite important phenomenon in thin laminate analysis (Fig. 6).

As the structural model gets closer to physical reality another experimental tests campaign will be necessary.

8 ACKNOWLEDGEMENTS

Deformation tests have been carried out in the Ship Structures Laboratory of DINAV, whose support is gratefully acknowledged. DIPTEM and DICAT labs of the University di Genova also supported the tests providing some instrumentation. Sail fabrics used for experiments were provided by Alessandro Castelli, Elvstrom-Sobstad.

9 BIBLIOGRAPHY

Arcaro, V. 2002. *Finite Element Analysis of 3D Isotropic Membrane Structures*. UNICAMP/FEC
Available on-line: http://www.arcaro.org/tension/index.htm

Belluzzi, O. 1966. *Scienza delle Costruzioni*. Bologna: Zanichelli editore,

Boote, D. and Caponnetto, M. 1991. A numerical approach to the design of sailing yacht masts. *The 10th Chesapeake Sailing Yacht Symposium*, Chesapeake, USA*: 59-81.*

Carassale, L. *Materiale didattico del corso di Scienza delle Costruzioni 2.* UNIGE
Available on-line http://www.dicat.unige.it/carassale/ Didattica/ SdC2Nav/MaterialeDidattico.html

Coiro, D. and Nicolosi, D and Scherillo, F. and Misto, U. 2002. Numerical and experimental aeroelastic analysis of sails. *High performance Yacht Design Conference*, Auckland, New Zealand.

Diaby, A. and Le van, A. and Wielgosz, C. 2006. Buckling and wrinkling of prestressed membranes.
Finite elements in Analysis and Design, volume 42: 992, 1001.

Fantini, F. 2004. P*restazioni di una vela. Una metodologia di calcolo.* Final Project. Available on-line:
http://etd.adm.unipi.it/theses/available/etd-02032004–112549/

Fukosawa, T and Katori, M. 1993. Numerical approach to aeroelastic flexible sails. *The 11th Chesapeake Sailing Yacht Symposium*, Chesapeake, USA: 87-105.

Graf, K. and Renzsch, H. 2006. RANSE Investigations of Downwind Sails and Integration Into Sailing Yacht Design Processes. *High performance Yacht Design Conference,* Auckland, New Zealand.

Graf, K. and Renzsch, H. 2008. FlexSail – A Fluid Structure interaction program for the investigation of Spinnaker. *High performance Sailing Yacht Conference*, Lorient, France.

Hauville, F. and Mounoury, S. and Roux, Y. and Astolfi, J. 2004. Equilibre dynamique d'une structure idéalement flexible dans un écoulement : application a la déformation des voiles. *Journées AUM AFM 2004*. Brest, France, 2004.

Heppel, P. 2002. Accuracy in Sail Simulations: Wrinkling and growing fast sails. *High performance Yacht Design Conference,* Auckland, New Zealand. Available on-line: www.peterheppel.com.

Lee, E. and Youn, S. 2006. Finite Elements analysis of wrinkling membrane structures with large deformation. *Elements in Analysis and Design*, vol. 42: 780, 791.

Levy, R. and Chen, C. and Lin, C and Yang, Y. 2004. Geometric stiffness of membranes using symbolic algebra. *Engineering Structures*, 6, vol. 26: 759-767.

Levy, R. and Spillers, W. 2003. *Analysis of Geometrically Nonlinear Structures.* Kluwer Academic Publishers, The Nederlands.

Li, J and Chan, S. 2004. An integrated analysis of membrane structures with flexible supporting frames. *Finite Elements in Analysis and Design*, 5-6, vol. 40: 529-540.

Paton, J. and Morvan, H. and Heppel, P. 2008. Fluid Structure interaction of Yacht Sails. *Hygh performance Sailing Yacht Conference*, Lorient, France.

Stanuszek, M. 2003. Finite elements analysis of large deformations of membranes with wrinkling. *Finite Elements in Analysis and Design,* vol 39: 599-618.

Tabarrok, B. and Qin, Z. 1992. Nonlinear analysis of tension structures. *Computer and Structures*, 5-6, vol. 45: 973–984.

Vernengo, G. 2008. Teoria e applicazione di un metodo a superficie portante per l'analisi aerodinamica di sistemi di vele. (in Italian) *Msc thesis, Università degli studi di Genova*